

Topological Structures in Two-Parameter-Dependent 2D Vector Fields

T. Weinkauff¹, H. Theisel², H.-C. Hege¹ and H.-P. Seidel²

¹ Zuse Institute Berlin (ZIB), Berlin, Germany — {weinkauff, hege}@zib.de

² MPI Informatik, Saarbrücken, Germany — {theisel, hpseidel}@mpi-sb.mpg.de

Abstract

In this paper we extract and visualize the topological skeleton of two-parameter-dependent vector fields. This kind of vector data depends on two parameter dimensions, for instance physical time and a scale parameter. We show that two important classes of local bifurcations – fold and Hopf bifurcations – build line structures for which we present an approach to extract them. Furthermore we show that new kinds of structurally stable local bifurcations exist for this data, namely fold-fold and Hopf-fold bifurcations. We present a complete classification of them. We apply our topological extraction method to analyze a number of two-parameter-dependent vector fields with different physical interpretations of the two additional dimensions.

Categories and Subject Descriptors (according to ACM CCS): I.3.3 [Computer Graphics]: Line and Curve Generation I.3.3 [Computer Graphics]: Picture/Image Generation

1. Introduction

Topological methods have become a standard tool in vector field visualization. Initially introduced as a visualization tool in [HH89], topological methods have been extended to higher order critical points [SKMR98], boundary switch points [dLvL99], and closed separatrices [WS01]. In addition, topological methods have been applied to smooth [WJE01], compress [LRR00, TRS03] and model [The02, WTHS04b] vector fields. The topology of 3D vector fields is visualized in [GLL91, LDG98, MBS*04, TWHS03, TWHS04a].

The main idea of topological methods is to segment the domain into areas of different flow behavior. To do so, critical points are extracted and classified. Starting from saddle points, separation curves/surfaces are integrated. The union of critical points and separatrices is called *topological skeleton*. Concerning vector fields $\mathbf{v}(\mathbf{x}, t)$, $\mathbf{x} \in \mathbb{R}^n$ depending on one parameter t (like e.g. time-dependent flows), critical points move with changing t . In fact, they form line structures in \mathbb{R}^{n+1} . Furthermore, critical points might appear or disappear at some t . Those births and deaths of critical points are called *fold bifurcations* and their occurrence changes the topological behavior of the field abruptly: two critical points

of opposite index collapse and disappear (or the other way around: a critical point appears and splits up into two critical points immediately). Knowing the locations of these events is a key to understanding the dynamics of the data. Another important structural change is denoted by a spiraling source changing to a spiraling sink or vice versa. This is called a *Hopf bifurcation*. Other types of local bifurcations (*Transcritical* and *Pitchfork bifurcation*) are possible, but structurally unstable [GH86] – we therefore do not treat them here.

This paper aims at extracting all locations of all critical points of vector fields $\mathbf{v}(\mathbf{x}, s, t)$ depending on two parameters. Critical points move with changing s and t and form surface structures now. Consequently, bifurcation points move as well and form line structures in \mathbb{R}^{n+2} . This creates new types of structurally stable bifurcations: births and deaths of fold or Hopf bifurcations themselves. We call them *fold-fold* and *Hopf-fold* bifurcations. Those events are isolated points in \mathbb{R}^{n+2} . See Table 1 for an overview of the dimensionality of topological features. A detailed introduction to the theory of local bifurcations of vector fields $\mathbf{v}(\mathbf{x}, s, t)$ can be found in [GH86]. In particular, local codimension two bifurcations are studied there. Guckenheimer and Holmes give a thor-

Feature	$\mathbf{v}(\mathbf{x}, t)$	$\mathbf{v}(\mathbf{x}, s, t)$
critical points	curves	surfaces
fold / Hopf bifurcations	points	curves
fold-fold / Hopf-fold bifurcations	<i>n/a</i>	points

Table 1: Dimensionality of topological features for vector fields depending on one or two parameters.

ough overview of the unfoldings of those bifurcations. The bifurcations we treat here fit into this scheme, but we distinguish between line-type and point-type bifurcations here. We do so, since this allows a better description of the structural changes inherent to the flow.

Vector fields of the form $\mathbf{v}(\mathbf{x}, s, t)$ can be found in a number of applications, two of them shall be mentioned here:

- **Multiscale Techniques:** Simplification [dLvL99] [TSH01a] and smoothing [BP02, KE05] lead to representations of vector fields at different scale levels. If the transition between them is smooth, we have a *scale-space* representation of the data, smoothly changing from the original data to a strongly simplified/smoothed version. If those techniques are applied to time-dependent flows, we end up with two-parameter-dependent vector fields.
- **Flow Optimization:** The flow around an airfoil is subject to large efforts in order to increase the desired lift and to reduce the parasitic drag. These performance enhancements are achieved by changing the geometry (aerodynamic design) of the airfoil and controlling separation using air injection. Both strategies introduce additional parameters like position and size of gurney flaps or amplitude and phase of air injection. Being able to extract the topology of flows with more than one parameter aids in understanding the intricate flow structures.

There is a large amount of research on extracting the topological skeleton of *one*-parameter-dependent vector fields $\mathbf{v}(\mathbf{x}, t)$, e.g., tracking critical points in time-dependent flows. Two main approaches exist: based on a local connection strategy exploiting the underlying grid [TSH01b, GTS04], or based on a stream line integration in a derived vector field – the so-called feature flow field (FFF) [TS03, WTHS05]. Both approaches have their strengths and weaknesses, making the choice of the appropriate one depending on the particular application.

In this paper we present an algorithm to extract the locations of all critical points of two-parameter-dependent vector fields $\mathbf{v}(\mathbf{x}, s, t)$. As part of this, we obtain the locations of fold and Hopf bifurcations as well as their births and deaths. Our algorithm is based on the feature flow field approach [TS03], which additionally provides the tools to completely classify *fold-fold* and *Hopf-fold* bifurcations. In this paper we treat 2D vector fields depending on two additional independent variables, i.e., vector fields of the form $\mathbf{v}(x, y, s, t)$.

The rest of the paper is organized as follows: section 2 recalls topological visualization approaches for time-dependent vector fields. Section 3 explains the visualization and critical point tracking in two-parameter-dependent fields. Section 4 presents an approach to tracking fold bifurcations. Section 5 introduces and classifies fold-fold bifurcations. Section 6 treats the tracking of Hopf bifurcations. Section 7 describes implementational details. In Section 8 we apply our technique to a number of test data sets, while conclusions are drawn in section 9.

2. One-Parameter-Dependent Vector Fields

Topological features of one-parameter-dependent vector fields (e.g. time-dependent) are well-understood in the visualization community. They can be classified into local and global features [TWHS05]. In this section, we give a short overview over local topological features, focusing on 2D fields. Given a 2D time-dependent vector field $\mathbf{v}(x, y, t)$, the locations of the critical points form line structures in the 3D space-time domain. To extract them, we use the FFF approach [TS03] which consists of two steps: first, a 3D vector field \mathbf{f} is constructed which fulfills the FFF property, i.e., the locations of the critical points of \mathbf{v} are stream lines of \mathbf{f} . This way, the tracking of critical points in \mathbf{v} can be carried out as a simple stream line integration of \mathbf{f} . [TS03] shows that

$$\mathbf{f}(x, y, t) = \begin{pmatrix} \det(\mathbf{v}_y, \mathbf{v}_t) \\ \det(\mathbf{v}_t, \mathbf{v}_x) \\ \det(\mathbf{v}_x, \mathbf{v}_y) \end{pmatrix}. \quad (1)$$

Second, a set of seeding points is extracted which guarantees that all locations of critical points of \mathbf{v} are covered by a stream line integration of \mathbf{f} . [TWHS05] shows that two classes of points together fulfill this: critical points of \mathbf{v} at the boundaries of the space-time domain, and the fold bifurcations.

Fold bifurcations can be found as the solutions of the following system of equations: $[\mathbf{v} = \mathbf{0}, \det(\mathbf{v}_x, \mathbf{v}_y) = 0]$. Two kinds of fold bifurcations exist: a birth and a death event. To distinguish them, we consider the sign of $(\nabla \mathbf{f} \cdot \mathbf{f})_3$ describing the third component of the directional derivative of \mathbf{f} in the direction of \mathbf{f} at the location of the fold bifurcation. If $(\nabla \mathbf{f} \cdot \mathbf{f})_3 > 0$, we have a birth event, while $(\nabla \mathbf{f} \cdot \mathbf{f})_3 < 0$ denotes a death event. $(\nabla \mathbf{f} \cdot \mathbf{f})_3 = 0$ gives a structurally unstable event (i.e., an event which disappears under adding noise to \mathbf{v}) and is not considered here. We call this discrimination of fold bifurcations into births or deaths the *BD classification*. In the following sections we will extend the BD classification for the use with two-parameter-dependent fields.

Hopf bifurcations can be extracted by solving the system $[\mathbf{v} = \mathbf{0}, \operatorname{div}(\mathbf{v}) = u_x + v_y = 0]$ for (x, y, t) and selecting all isolated solutions with a positive Jacobian of \mathbf{v} .

To visualize the locations of the critical points, we consider the 3D space-time domain. Figure 1a gives an example

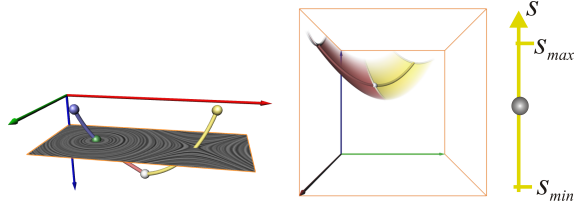


Figure 1: (a) Critical points in a one-parameter-dependent vector field including a fold and a Hopf bifurcation (gray / green point). (b) Visualizing a two-parameter-dependent vector field by interactively moving s .

showing the vector field at a certain time using a LIC image. In addition, the paths of the critical points are shown as colored 3D curves: a yellow curve denotes a moving saddle point, a red/blue curve denotes moving sources/sinks. The green point is a Hopf bifurcation, while the gray point shows the location of a fold bifurcation. The red/green coordinate axes correspond to spatial directions, while the blue axis denotes time.

3. Two-Parameter-Dependent Vector Fields

Two-parameter-dependent 2D vector fields shall be written

$$\mathbf{v}(\mathbf{x}, s, t) = \mathbf{v}(x, y, s, t) = \begin{pmatrix} u(x, y, s, t) \\ v(x, y, s, t) \end{pmatrix} \quad (2)$$

where x, y represent the spatial and s, t denote the additional dimensions of the domain. In fact, s can be considered as the scale-space parameter while t serves as the physical time parameter, but other interpretations of s, t are possible as well. For the further explanation of the concepts, we distinguish two domains of \mathbf{v} : the 2D spatial subdomain D with fixed s and t , and the full 4D domain \tilde{D} . For the sake of simplicity, we consider $D = [x_{min}, x_{max}] \times [y_{min}, y_{max}]$ and mention that our algorithms work for more general domain boundaries as well. Furthermore, we choose $\tilde{D} = D \times [s_{min}, s_{max}] \times [t_{min}, t_{max}]$. In the following we write $\mathbf{v}, \mathbf{w}, \dots$ for 2D vector fields but $\tilde{\mathbf{v}}, \tilde{\mathbf{w}}, \dots$ for 4D vector fields in \tilde{D} .

The locations of the critical points of \mathbf{v} build surface structures in \tilde{D} . Before we discuss their extraction (section 3.2), we explain our approaches to visualizing them (section 3.1).

3.1. Visualizing Critical Points in \tilde{D}

4D surface structures are challenging objects for an expressive visual representation. We use three approaches:

- Interactively changing s and t : a point (s, t) is interactively moved in the domain $[s_{min}, s_{max}] \times [t_{min}, t_{max}]$, and the topological skeleton of \mathbf{v} at (s, t) is visualized. Figure 2 does so for 5 different locations (s, t) . We refer to this as (x, y) -visualization.

- Interactively changing s : for a given location s , \mathbf{v} is interpreted and visualized as one-parameter-dependent field $\mathbf{v}(\mathbf{x}, t)$. In addition, faded-out surfaces starting from the zero-lines denote the situation in the direct s -past/future. Figure 1(right) gives an illustration. There, the topological skeleton for a fixed s consists of a moving saddle (yellow curve), a moving source (red curve), and a fold bifurcation (gray point). When moving forward/backward in s , these features change shape and location. This is represented by the faded-out red/yellow surfaces for the moving source/saddle, and by the faded-out gray line starting from the fold bifurcation. To avoid cluttered visualizations, the faded lines/surfaces can be switched off. We call this a (x, y, t) -visualization.
- Interactively changing t : similar to the previous approach, but with a one-parameter-dependent visualization of $\mathbf{v}(\mathbf{x}, s)$ for a fixed t . We call this a (x, y, s) -visualization.

Note that although the two latter visualization approaches give more insight into the topological behavior of \mathbf{v} , the first one is the only one which straightforwardly extends to 3D vector fields depending on two parameters. In all figures, we use the following colors for the coordinate axes: red= x , green= y , yellow= s , blue= t .

3.2. Tracking Critical Points in \tilde{D}

Different approaches to tracking critical points of \mathbf{v} in \tilde{D} are possible. A Marching-Cubes- or Marching-Tetrahedra-like approach can be applied if the underlying grid provides a piecewise (quadri-)linear vector field. [BP02] uses a similar approach to tracking 3D vortex core lines over time. Here we use a FFF-based approach ending up in a 4D stream surface integration. We do so, because the FFF approach is independent of an underlying grid, and it provides the tool to detect and classify bifurcations in \tilde{D} (section 5). Since the searched structures are surfaces in \tilde{D} , we need two FFF's to track them. Following [TS03] we use

$$\tilde{\mathbf{f}} = \begin{pmatrix} \det(\mathbf{v}_y, \mathbf{v}_s) \\ \det(\mathbf{v}_s, \mathbf{v}_x) \\ \det(\mathbf{v}_x, \mathbf{v}_y) \\ 0 \end{pmatrix}, \quad \tilde{\mathbf{g}} = \begin{pmatrix} \det(\mathbf{v}_y, \mathbf{v}_t) \\ \det(\mathbf{v}_t, \mathbf{v}_x) \\ 0 \\ \det(\mathbf{v}_x, \mathbf{v}_y) \end{pmatrix}. \quad (3)$$

$\tilde{\mathbf{f}}$ tracks a critical point in s (keeping t constant), while $\tilde{\mathbf{g}}$ tracks the critical points in t (keeping s constant). We give the following algorithm to get all seeding structures:

- I Extract all critical points on the domain boundaries of \tilde{D} , i.e., all points (x, y, s, t) with $[\mathbf{v}(x, y, s, t) = 0, E]$ and E is one of the 8 expressions $x = x_{min}, x = x_{max}, y = y_{min}, y = y_{max}, s = s_{min}, s = s_{max}, t = t_{min}, t = t_{max}$. Here, the FFF approach of Section 2 can be applied.
- II Extract all locations of fold bifurcations in \tilde{D} . This can be done using the new FFF based approach presented in the following section.

This choice of seeding structures is a direct generalization of the one-parameter case [TWH05]. Both I and II yield

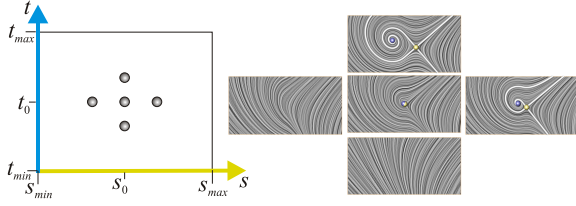


Figure 2: A (BB) fold bifurcation at (\mathbf{x}_0, s_0, t_0) : shown are the topological skeleton and the LIC images of \mathbf{v} at (s_0, t_0) and $(s_0 \pm \varepsilon, t_0 \pm \varepsilon)$. The arrangement of the LIC images (right) corresponds to the points in the (s, t) -diagram (left). Starting from (s_0, t_0) moving forward either in s or in t creates a splitting of the critical point at (s_0, t_0) .

line structures. Depending on whether one wants to track the critical points in s or in t one needs to apply a stream surface integration using $\tilde{\mathbf{f}}$ or $\tilde{\mathbf{g}}$ respectively. The union of both results yields all locations of all critical points of \mathbf{v} in \tilde{D} .

4. Tracking Fold Bifurcations

For one-parameter-dependent vector fields, fold bifurcations are isolated points serving as seeding structures to track the critical points. In two-parameter-dependent vector fields they build line structures in \tilde{D} . Fold bifurcations occur at points in \tilde{D} fulfilling

$$[\mathbf{v} = \mathbf{0}, \det(\mathbf{v}_x, \mathbf{v}_y) = 0]. \quad (4)$$

Since $\tilde{\mathbf{f}}.3 = \tilde{\mathbf{g}}.4$ in (3), fold bifurcations occur simultaneously in s and in t . This means that depending on the signs of $(\nabla \tilde{\mathbf{f}} \cdot \tilde{\mathbf{f}}).3$ and $(\nabla \tilde{\mathbf{g}} \cdot \tilde{\mathbf{g}}).4$, a fold bifurcation in \tilde{D} can have 4 different BD classifications: (BB), (BD), (DB), (DD), where the first letter denotes the BD classification in s and the second does so in t . Figure 2 illustrates a (BB) fold bifurcation. To track the locations of fold bifurcations in \tilde{D} , we apply the FFF approach again. Its two parts are explained in the following two sections.

4.1. FFF for Tracking Fold Bifurcations

Let $\tilde{\mathbf{h}}$ be the 4D vector field in question to track fold bifurcations in \tilde{D} . Using the abbreviation

$$d = \det(\mathbf{v}_x, \mathbf{v}_y), \quad (5)$$

$\tilde{\mathbf{h}}$ has to point into the direction where \mathbf{v} and d remain constant in a local first order approximation. This means that $\tilde{\mathbf{h}}$ has to fulfill

$$[\tilde{\mathbf{h}} \perp \nabla u, \tilde{\mathbf{h}} \perp \nabla v, \tilde{\mathbf{h}} \perp \nabla d] \quad (6)$$

with

$$\nabla u = \begin{pmatrix} u_x \\ u_y \\ u_s \\ u_t \end{pmatrix}, \quad \nabla v = \begin{pmatrix} v_x \\ v_y \\ v_s \\ v_t \end{pmatrix} \quad (7)$$

$$\nabla d = \begin{pmatrix} d_x \\ d_y \\ d_s \\ d_t \end{pmatrix} = \begin{pmatrix} \det(\mathbf{v}_{xx}, \mathbf{v}_y) + \det(\mathbf{v}_x, \mathbf{v}_{xy}) \\ \det(\mathbf{v}_{xy}, \mathbf{v}_y) + \det(\mathbf{v}_x, \mathbf{v}_{yy}) \\ \det(\mathbf{v}_{xs}, \mathbf{v}_y) + \det(\mathbf{v}_x, \mathbf{v}_{ys}) \\ \det(\mathbf{v}_{xt}, \mathbf{v}_y) + \det(\mathbf{v}_x, \mathbf{v}_{yt}) \end{pmatrix} \quad (8)$$

Equation (6) describes a linear system which gives a unique solution for $\tilde{\mathbf{h}}$ (except for scaling):

$$\tilde{\mathbf{h}} = \begin{pmatrix} \det(\nabla u, \nabla v, \nabla d, \mathbf{i}_1) \\ \det(\nabla u, \nabla v, \nabla d, \mathbf{i}_2) \\ \det(\nabla u, \nabla v, \nabla d, \mathbf{i}_3) \\ \det(\nabla u, \nabla v, \nabla d, \mathbf{i}_4) \end{pmatrix} \quad (9)$$

where $\mathbf{i}_1, \dots, \mathbf{i}_4$ are the columns of the 4×4 unit matrix. Equation (9) can be rewritten as

$$\tilde{\mathbf{h}} = \begin{pmatrix} -d_y \det(\mathbf{v}_s, \mathbf{v}_t) + d_s \det(\mathbf{v}_y, \mathbf{v}_t) - d_t \det(\mathbf{v}_y, \mathbf{v}_s) \\ +d_x \det(\mathbf{v}_s, \mathbf{v}_t) - d_s \det(\mathbf{v}_x, \mathbf{v}_t) + d_t \det(\mathbf{v}_x, \mathbf{v}_s) \\ -d_x \det(\mathbf{v}_y, \mathbf{v}_t) + d_y \det(\mathbf{v}_x, \mathbf{v}_t) - d_t d \\ +d_x \det(\mathbf{v}_y, \mathbf{v}_s) - d_y \det(\mathbf{v}_x, \mathbf{v}_s) + d_s d \end{pmatrix}. \quad (10)$$

4.2. Starting Points for Integrating $\tilde{\mathbf{h}}$

In order to compute the starting points for integrating $\tilde{\mathbf{h}}$, we have to compute the intersection points of the paths of the fold bifurcations with the 8 boundary surfaces of \tilde{D} , i.e., locations with

$$[(4), E] \quad (11)$$

and E is one of the 8 expressions $x = x_{min}, x = x_{max}, y = y_{min}, y = y_{max}, s = s_{min}, s = s_{max}, t = t_{min},$ or $t = t_{max}$. Solving each of those 8 systems is equivalent to finding isolated critical points in a 3D vector field. In addition, we have to extract inner bifurcation points where fold bifurcations appear or disappear. We call them *fold-fold bifurcations* and treat them in the next section.

5. Fold-fold Bifurcations

A fold-fold bifurcation is the event of collapsing and disappearing of two fold bifurcations while moving forward either in s or in t (or the reverse process: the appearance and splitting of two fold bifurcations). Fold-fold bifurcations occur at points with vanishing third or fourth component of $\tilde{\mathbf{h}}$.

There are three kinds of structurally stable fold-fold bifurcations. An *s-fold-fold* bifurcation is characterized by

$$[(4), \tilde{\mathbf{h}}.3 = 0, \tilde{\mathbf{h}}.4 \neq 0]. \quad (12)$$

A *t-fold-fold* bifurcation is characterized by

$$[(4), \tilde{\mathbf{h}}.3 \neq 0, \tilde{\mathbf{h}}.4 = 0]. \quad (13)$$

An *s-t-fold-fold* bifurcation is characterized by

$$[(4), \tilde{\mathbf{h}}.3 = 0, \tilde{\mathbf{h}}.4 = 0]. \quad (14)$$

In order to show that structurally stable solutions in \tilde{D} for all

three kinds of bifurcations exist, we note that (4) implies that \mathbf{v}_x and \mathbf{v}_y are parallel, i.e., $\mathbf{v}_y = \lambda \mathbf{v}_x$ for a certain λ . Inserting this and $d = 0$ into (10) gives

$$\begin{aligned}\tilde{\mathbf{h}}.3 &= -(\lambda d_x - d_y) \det(\mathbf{v}_x, \mathbf{v}_t) \\ \tilde{\mathbf{h}}.4 &= (\lambda d_x - d_y) \det(\mathbf{v}_x, \mathbf{v}_s).\end{aligned}\quad (15)$$

This means that an s -fold-fold bifurcation occurs at $[(4), \det(\mathbf{v}_x, \mathbf{v}_t) = 0]$ which is equivalent to

$$[\mathbf{v} = \mathbf{0}, \tilde{\mathbf{g}} = \mathbf{0}]. \quad (16)$$

A t -fold-fold bifurcation occurs at $[(4), \det(\mathbf{v}_x, \mathbf{v}_s) = 0]$ which is equivalent to

$$[\mathbf{v} = \mathbf{0}, \tilde{\mathbf{f}} = \mathbf{0}]. \quad (17)$$

An s - t -fold-fold bifurcation occurs at $[(4), \lambda d_x - d_y = 0]$ which is equivalent to

$$[\mathbf{v} = \mathbf{0}, d_y \mathbf{v}_x = d_x \mathbf{v}_y]. \quad (18)$$

s -fold-fold and t -fold-fold bifurcations can be further classified by applying well-known approaches from vector field topology: an eigen-analysis of the Jacobian at the critical point. For an s -fold-fold, we consider the eigenvalues of $\nabla \tilde{\mathbf{g}}$ at the bifurcation. Appendix 10 shows that they have the form $0, 0, -\sqrt{r_s}, \sqrt{r_s}$ where r_s is a certain real number. This gives the following classification: an s -fold-fold with $r_s < 0$ gives a *closed collapse bifurcation*: while moving forward/backward in s , a closed zero-line of \mathbf{v} becomes smaller, collapses to a point, and disappears. For $r_s > 0$ we obtain a *saddle bifurcation*: while moving forward/backward in s , two branches of the zero-curves of \mathbf{v} move toward each other until they intersect and make the two fold bifurcations disappear. The case $r_s = 0$ gives a structurally unstable event and is not considered here.

The classification of a t -fold-fold bifurcation into saddle and closed collapse works in a similar way. Here we compute the eigenvalues of $\nabla \tilde{\mathbf{f}}$ which turn out to have the structure $0, 0, -\sqrt{r_t}, \sqrt{r_t}$ for a certain real number r_t . Then $r_t > 0$ gives a saddle bifurcation and $r_t < 0$ gives a closed collapse bifurcation.

Figures 3a–3c illustrate a number of fold-fold bifurcations. Figure 3a shows an s -fold-fold saddle bifurcation. The first row shows the visualization at 5 consecutive steps in s . Throughout the entire figure 3, the bifurcations occur in the third picture of every row. The same field as in the first row is shown in the second row of figure 3a, but now with interactively changing t . In fact, the third image of the first row and the third image of the second row are the visualizations at the same location (s, t) in which the bifurcation occurs. As we can see in the second row, no collapsing/splitting of the fold bifurcation occurs at an s -fold-fold bifurcation if moving in t . Figure 3b shows the same visualization for a t -fold-fold closed collapse bifurcation. Figure 3c shows an example of an s - t -fold-fold bifurcation. The two rows of this

	s -fold-fold	t -fold-fold	s - t -fold-fold
saddle	$\tilde{\mathbf{f}} \neq \mathbf{0}, \tilde{\mathbf{g}} = \mathbf{0}$ $r_s > 0$	$\tilde{\mathbf{f}} = \mathbf{0}, \tilde{\mathbf{g}} \neq \mathbf{0}$ $r_t > 0$	$d_y \mathbf{v}_x = d_x \mathbf{v}_y$
closed collapse	$\tilde{\mathbf{f}} \neq \mathbf{0}, \tilde{\mathbf{g}} = \mathbf{0}$ $r_s < 0$	$\tilde{\mathbf{f}} = \mathbf{0}, \tilde{\mathbf{g}} \neq \mathbf{0}$ $r_t < 0$	

Table 2: The five cases of fold-fold bifurcations.

s -fold-fold	t -fold-fold	s - t -fold-fold
(BB) \leftrightarrow (BD)	(BB) \leftrightarrow (DB)	(BB) \leftrightarrow (DD)
(DB) \leftrightarrow (DD)	(BD) \leftrightarrow (DD)	(BD) \leftrightarrow (DB)

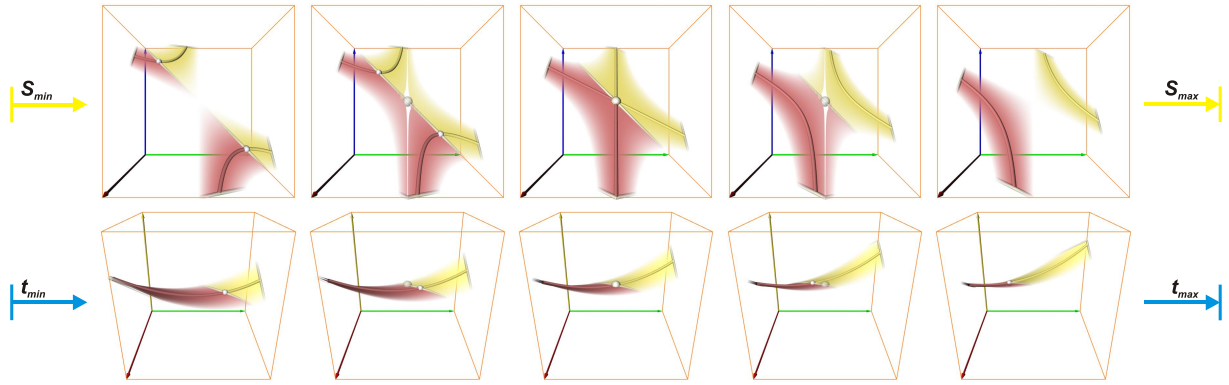
Table 3: Classification of fold-fold bifurcations wrt. the BD classification of the collapsing/splitting fold bifurcations.

figure show that the splitting/collapsing of the fold bifurcation occurs while moving forward in both s and t .

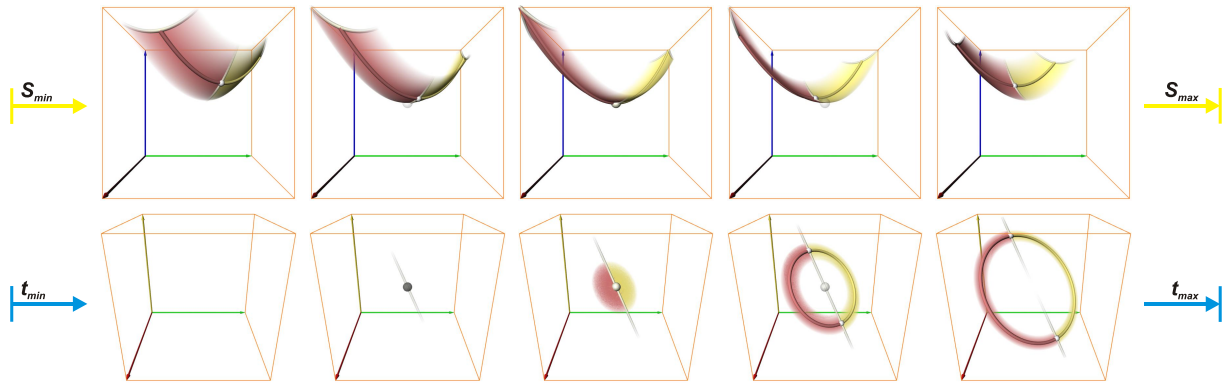
Table 2 summarizes the conditions for the 5 possible cases of fold-fold bifurcations. Each of the cases occurs at structurally stable locations in \tilde{D} with $\mathbf{v} = \mathbf{0}$ and the additional conditions as shown in the table. A rather similar classification of moving line structures as considered here was obtained in [TSW*05] in a different context: the tracking of vortex core lines in 3D time-dependent vector fields. Note that - similar to s -fold-fold and t -fold-fold bifurcations, the possible bifurcations of moving vortex core lines are also called saddle and closed collapse.

Each of the 5 fold-fold bifurcations can be further classified concerning their BD classification. In fact, an s -fold-fold and a t -fold-fold can be either a birth or a death event of two fold bifurcations. This means that the BD classification of an s -fold-fold and a t -fold-fold bifurcation is either (B) or (D). For an s - t -fold-fold the BD classification can be considered for both s and t , yielding 4 cases for the BD classification: (BB), (BD), (DB), (DD). This means that by adding a BD classification to the 5 fold-fold bifurcations, we end up with 12 different cases of fold-fold bifurcations. For example, the complete classification of the fold-fold bifurcations in figure 3a is (D)- s -fold-fold saddle, figure 3b shows a (B)- t -fold-fold closed collapse, and figure 3c shows a (DB)- s - t -fold-fold.

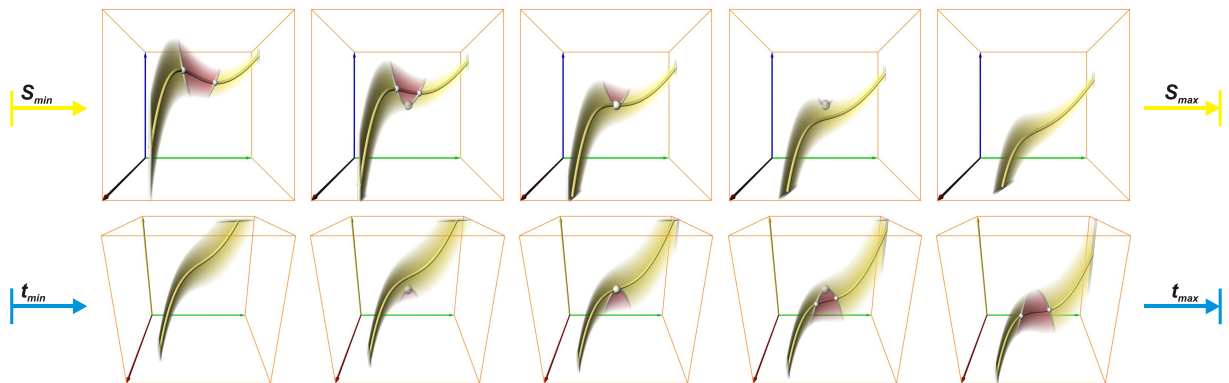
Fold-fold bifurcations can also be classified from another point of view: from the BD classification of the two collapsing/splitting fold bifurcations. If for instance a (BB) fold bifurcation collapses with a (BD) fold, we write (BB) \leftrightarrow (BD) for the fold-fold bifurcation. Table 3 shows the relation to the above-mentioned classification. Note that this classification is different to the BD classification of fold-fold bifurcations mentioned above. Here, we consider the BD classifications of the collapsing fold bifurcations, while in the other case



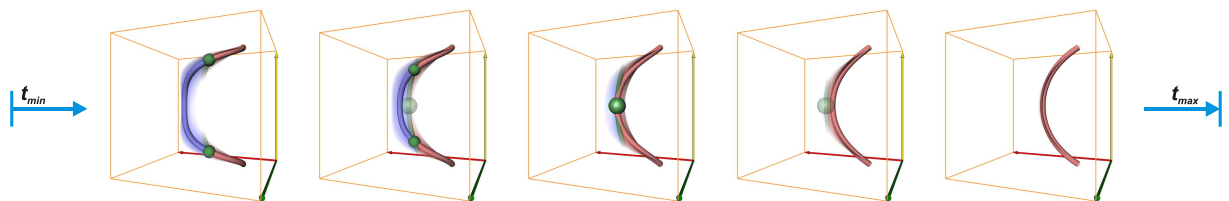
(a) *s*-fold-fold saddle bifurcation.



(b) *t*-fold-fold closed collapse bifurcation.



(c) *s-t*-fold-fold bifurcation.



(d) *t*-Hopf-fold bifurcation.

Figure 3: Fold-fold and Hopf-fold bifurcations.

we consider the BD classification of the fold-fold bifurcations themselves.

6. Tracking Hopf Bifurcations

A Hopf bifurcation, i.e., an event where a spiraling source changes to a spiraling sink or vice versa, occurs at

$$[\mathbf{v} = \mathbf{0}, \operatorname{div}(\mathbf{v}) = 0] \quad (19)$$

together with $\det(\mathbf{v}_x, \mathbf{v}_y) > 0$. Similar to fold bifurcations, Hopf bifurcations build line structures in \tilde{D} . For tracking them, we use again the FFF approach. In fact, we track all parts fulfilling (19) and subsequently eliminate all parts of the resulting lines with $\det(\mathbf{v}_x, \mathbf{v}_y) \leq 0$. As part of the tracking, we consider the events of collapsing/splitting two Hopf bifurcations: the Hopf-fold bifurcations.

6.1. FFF for Tracking Hopf Bifurcations

Let $\tilde{\mathbf{k}}$ be the FFF in question for tracking Hopf bifurcations. Using the abbreviation

$$e = \operatorname{div}(\mathbf{v}) = u_x + v_y, \quad (20)$$

$\tilde{\mathbf{k}}$ has to fulfill

$$[\tilde{\mathbf{k}} \perp \nabla u, \tilde{\mathbf{k}} \perp \nabla v, \tilde{\mathbf{k}} \perp \nabla e]. \quad (21)$$

which is a linear system with a unique solution for $\tilde{\mathbf{k}}$ (except for scaling):

$$\tilde{\mathbf{k}} = \begin{pmatrix} \det(\nabla u, \nabla v, \nabla e, \mathbf{i}_1) \\ \det(\nabla u, \nabla v, \nabla e, \mathbf{i}_2) \\ \det(\nabla u, \nabla v, \nabla e, \mathbf{i}_3) \\ \det(\nabla u, \nabla v, \nabla e, \mathbf{i}_4) \end{pmatrix}. \quad (22)$$

Note that the last two components of $\tilde{\mathbf{k}}$ are

$$\tilde{\mathbf{k}}.3 = -e_x \det(\mathbf{v}_y, \mathbf{v}_t) + e_y \det(\mathbf{v}_x, \mathbf{v}_t) - e_t d \quad (23)$$

$$\tilde{\mathbf{k}}.4 = +e_x \det(\mathbf{v}_y, \mathbf{v}_s) - e_y \det(\mathbf{v}_x, \mathbf{v}_s) + e_s d. \quad (24)$$

The starting points for integrating $\tilde{\mathbf{k}}$ are the Hopf bifurcations at the boundary of \tilde{D} , and the Hopf-fold bifurcations.

6.2. Hopf-fold Bifurcations

There are two kinds of Hopf-fold bifurcations. An *s-Hopf-fold* is the event of collapsing two Hopf bifurcations while moving forward/backward in *s*. They occur at structurally stable isolated points with

$$[(19), \tilde{\mathbf{k}}.3 = 0]. \quad (25)$$

Their detection is equivalent to finding critical points in 4D vector fields. At a *t-Hopf-fold* bifurcations, two Hopf bifurcations collapse while moving forward/backward in *t*. The condition for them is

$$[(19), \tilde{\mathbf{k}}.4 = 0]. \quad (26)$$

Figure 3d illustrates a Hopf-fold bifurcation.

7. Implementational Details

To implement our topological method, a number of problems have to be solved which are addressed in this section.

Some algorithms described in sections 2–6 are equivalent to finding isolated critical points in *n*-dimensional vector fields ($n = 2, 3, 4$ here). The detection of critical points is a numerically challenging problem itself. We use a recursive subdivision approach which we explain at a 3D example, but it works in 2D or 4D in a similar way. To check whether a 3D vector field \mathbf{w} has critical points inside a box-shaped cell *C*, we inspect the components of \mathbf{w} at all 8 vertices of *C*. If one of the components is positive at all vertices (or if one component is negative at all vertices), no critical point inside *C* is possible. Otherwise we apply a recursive octree subdivision of *C* until its size is smaller than a certain threshold. This method guarantees to find all critical points if \mathbf{w} is piecewise trilinear and the initial cells correspond to the underlying grid. However, in most of the applications in sections 2–6 certain derivatives of \mathbf{v} are involved, making it necessary to start with smaller initial search cells than the given grid. Another problem is the performance. Especially for $n = 4$ the algorithm may become rather time-consuming, making for instance the direct search for isolated fold-fold and Hopf-fold bifurcations applicable only for very small data sets. Therefore, in our applications we extract fold bifurcations on the boundaries of \tilde{D} and restrict the search for fold-fold bifurcations to the stream lines of $\tilde{\mathbf{h}}$ starting from these folds at the boundary.

Our method involves higher order derivatives of the 2D vector field \mathbf{v} . The data we consider here is given on regular grids for which we used the quadratic super spline interpolation from [RZNS04]. This way, a C^1 continuous \mathbf{v} gives C^0 continuous $\tilde{\mathbf{h}}$ and $\tilde{\mathbf{k}}$.

Our approach is strongly based upon a numerical stream line integration in *n*-dimensional ($n = 2, 3, 4$) vector fields. Our implementation uses a 4th-order Runge-Kutta integration with adaptive step size control. Special care has to be taken at the grid boundaries. Since $\tilde{\mathbf{h}}$ and $\tilde{\mathbf{k}}$ are only C^0 continuous, the step size close to the grid boundary has to be adapted to hit the boundary. For this point, the next integration step in the next cell can be carried out.

One of the main problems of the FFF approach is that it has to keep the complete vector field in main memory. Two-parameter-dependent vector fields may grow too large in size even for the memory of high-end workstations. In this case, out-of-core modifications of the FFF approach can be applied [WTHS05].

8. Applications

In this section, we apply our topological methods to a number of test data sets.

Figures 4–5 show the visualization of a random data set

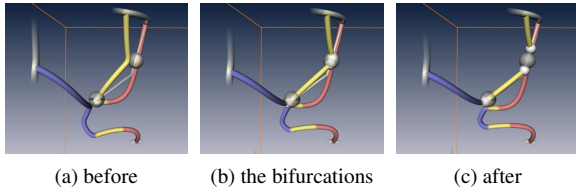


Figure 4: Noise data set: two saddle bifurcations.

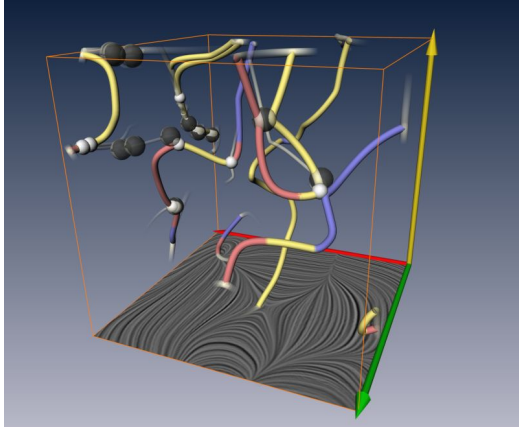


Figure 5: Noise data set: overview.

on a 4^4 grid. Random vector fields are used as a proof-of-concept since they contain the maximal amount of topological information. Figure 5 shows an overview in (x, y, s) -visualization. We see the paths of the critical points at a certain time t and at the boundaries of \tilde{D} . Figure 4 shows a detail of the data: two s -fold-fold saddle bifurcations in (x, y, s) -visualization.

Figures 6–7 show the visualization of a 2D time-dependent vector field $\mathbf{v}(x, y, t)$ describing the flow behind a 2D cylinder. The data set was kindly provided by Gerd Mutschke (FZ Rossendorf) and Bernd R. Noack (TU Berlin). This flow exhibits periodic vortex shedding leading to the well known von Kármán vortex street. This phenomenon plays an important role in many industrial applications, like mixing in heat exchangers or mass flow measurements with vortex counters. However, this vortex shedding can lead to undesirable periodic forces on obstacles, like chimneys, buildings, bridges and submarine towers. The original version of this non-compressible flow does not contain critical points (except for two directly behind the cylinder). The right-hand image of figure 7a illustrates it at a certain time t . In order to make topological methods applicable, a constant vector field can be subtracted which corresponds to an observer moving with the flow. In order to study the influence of the subtracted part, we apply our topological analysis: if the average flow of the original field is approximately $(1, 0)^T$ as for the given data set,

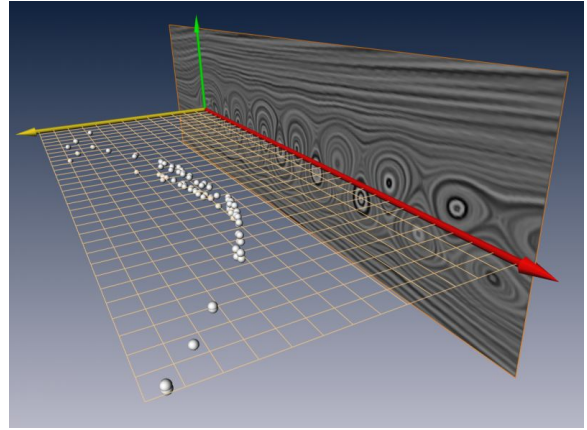


Figure 6: Cylinder flow: all fold-fold bifurcations in (x, y, s) -visualization.

we subtract the constant vector field $(1 - s) \cdot (1, 0)^T$ with $s \in [0, 1]$. This gives the two-parameter-dependent vector field $\mathbf{v}(x, y, s, t) = \mathbf{v}(x, y, t) - (1 - s) \cdot (1, 0)^T$. Figure 7a already shows for one particular t that increasing s from 0 to 1 will make the critical points collapse and disappear. Figures 7b–7e show $\mathbf{v}(x, y, t)$ at 4 different s -values. Each of the images shows the moving critical points in t as yellow (saddle) and green (center) 3D curves. The larger s gets, the fewer moving critical points are present. Figures 7b–7e also show that the disappearance of the moving critical points does not start from one of the boundaries of D but at a certain area located downstream of the cylinder. To analyze this further, we switch to a (x, y, s) -visualization as shown in figure 6. Here we visualized all detected fold-fold bifurcations. We can clearly see the parabola-like shape whose minimum denotes the location where – when moving forward in s – the first moving critical points disappear. For this data set we detected 92 fold-fold bifurcations, all of them are s -fold-fold saddle bifurcations. The computing time was in the range of several hours for detecting the paths of the critical points of \mathbf{v} at the boundaries of \tilde{D} . However, if this computation is carried out once, the extraction of a skeleton for a particular s/t is possible in less than a second on a current PC based system.

Figure 8 shows the visualization of the wind components of the Hurricane Isabel data set from the IEEE Visualization 2004 contest. It was produced by the Weather Research and Forecast (WRF) model, courtesy of NCAR and the U.S. National Science Foundation (NSF). Although this is a one-parameter-dependent 3D vector field $\mathbf{v}(x, y, z, t) = (u, v, w)^T$, the main flow takes place in u - and v -direction. By neglecting the w -component and setting $z = s$, we obtain a two-parameter-dependent 2D field from which we analyze the first half of the original 48 time steps. Figures 8a–8d show the (x, y, s) -visualization for different t -steps. We can clearly

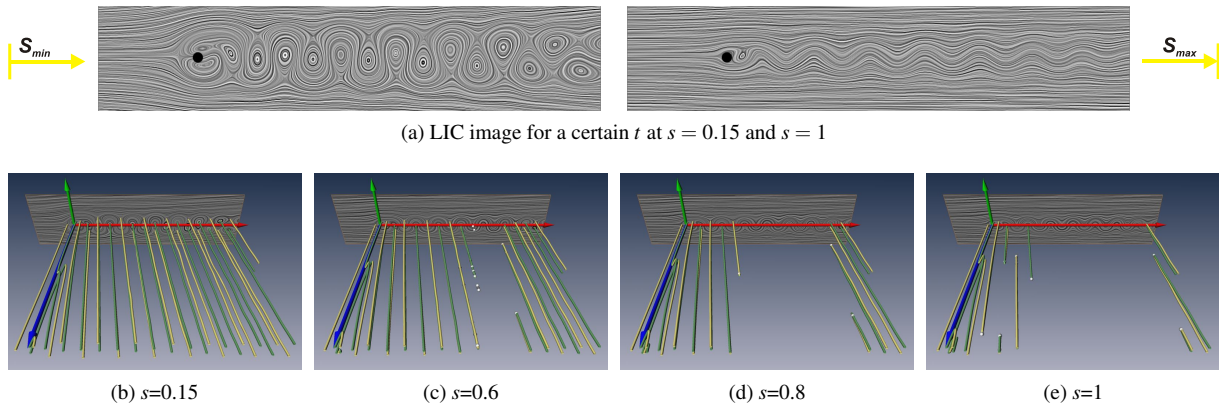


Figure 7: Flow behind a circular cylinder: s controls the subtracted constant field, t is the physical time parameter. (a) LIC image for a certain t and two different s , (b)–(e) (x, y, t) -visualization for 4 different s .

see the dominating moving critical point (green line) changing its location while moving forward in t . Also, for high s -values the dominating critical point tends to have a fold bifurcation with a moving saddle (yellow). Figure 8e shows the top view at $t=19$. Figure 8f shows the location of the dominating critical point of \mathbf{v} at the boundary $s = s_{min}$ of \tilde{D} (white line). Note that this line serves as the seeding structure to integrating the moving critical points at different t -values. Figure 8f also shows the moving critical point at $t = 4$ and $t = 25$.

9. Conclusions and Future Work

In this paper, we made the following contributions:

- We introduced a topology-based visualization approach for two-parameter-dependent 2D vector fields.
- As part of this, we presented an algorithm to tracking fold bifurcations and Hopf bifurcations in the 4D domain.
- We discussed local bifurcations introduced by the additional parameter: fold-fold and Hopf-fold bifurcations. Based on an analysis of the underlying feature flow fields, we gave a complete classification of them. We identified 5 classes of fold-fold and 2 classes of Hopf-fold bifurcations (not including their BD classification).
- We applied the topological analysis to a number of test data sets which cover different physical interpretations of the two additional dimensions.

The most challenging issue for future research is the extension of our approach from 2D to 3D two-parameter-dependent vector fields. While most of the topological concepts extend straightforwardly, the main problem seems to be an adequate visual representation of the resulting 5D features.

Acknowledgments

We thank Bernd R. Noack for the fruitful discussions and the supply of the cylinder data set which was kindly provided by Gerd Mutschke (FZ Rossendorf). We thank Jan Sahner, Nathalie Teuber and Jan Reininghaus for their sharp thoughts and code. We thank Natascha Sauber for her help with the Hurricane Isabel data set. All visualizations in this paper have been created using AMIRA – a system for advanced visual data analysis [SWH05] (see <http://amira.zib.de/>).

References

- [BP02] BAUER D., PEIKERT R.: Vortex tracking in scale space. In *Data Visualization 2002. Proc. VisSym 02* (2002), pp. 233–240.
- [dLvL99] DE LEEUW W., VAN LIERE R.: Collapsing flow topology using area metrics. In *Proc. IEEE Visualization '99* (1999), pp. 149–354.
- [GH86] GUCKENHEIMER J., HOLMES P.: *Nonlinear Oscillations, Dynamical Systems, and Bifurcations of Vector Fields*, 2nd ed. Springer, 1986.
- [GLL91] GLOBUS A., LEVIT C., LASINSKI T.: A tool for visualizing the topology of three-dimensional vector fields. In *Proc. IEEE Visualization '91* (1991), pp. 33–40.
- [GTS04] GARTH C., TRICOCHE X., SCHEUERMANN G.: Tracking of vector field singularities in unstructured 3D time-dependent datasets. In *Proc. IEEE Visualization 2004* (2004), pp. 329–336.
- [HH89] HELMAN J., HESSELINK L.: Representation and display of vector field topology in fluid flow data sets. *IEEE Computer* 22, 8 (August 1989), 27–36.
- [KE05] KLEIN T., ERTL T.: Scale-space tracking of critical points in 3D vector fields. In *Topo-In-Vis 2005* (2005). (submitted).
- [LDG98] LÖFFELMANN H., DOLEISCH H., GRÖLLER E.: Visualizing dynamical systems near critical points. In *Spring Conference on Computer Graphics and its Applications* (Budmerice, Slovakia, 1998), pp. 175–184.
- [LRR00] LODHA S., RENTERIA J., ROSKIN K.: Topology preserving compression of 2D vector fields. In *Proc. IEEE Visualization 2000* (2000), pp. 343–350.
- [MBS*04] MAHROUS K., BENNETT J., SCHEUERMANN G., HAMANN B., JOY K.: Topological segmentation in three-dimensional vector fields. *IEEE Transactions on Visualization and Computer Graphics* 10, 2 (2004), 198–205.
- [RZNS04] ROESSL C., ZEILFELDER F., NUERNBERGER G., SEIDEL H.-P.: Reconstruction of volume data with quadratic super splines. *IEEE Trans. Visualization and Computer Graphics* 10 (2004), 397–409.
- [SKMR98] SCHEUERMANN G., KRÜGER H., MENZEL M., ROCKWOOD A.: Visualizing non-linear vector field topology. *IEEE Transactions on Visualization and Computer Graphics* 4, 2 (1998), 109–116.
- [SWH05] STALLING D., WESTERHOFF M., HEGE H.-C.: Amira: A highly interactive system for visual data analysis. *The Visualization Handbook* (2005), 749–767.

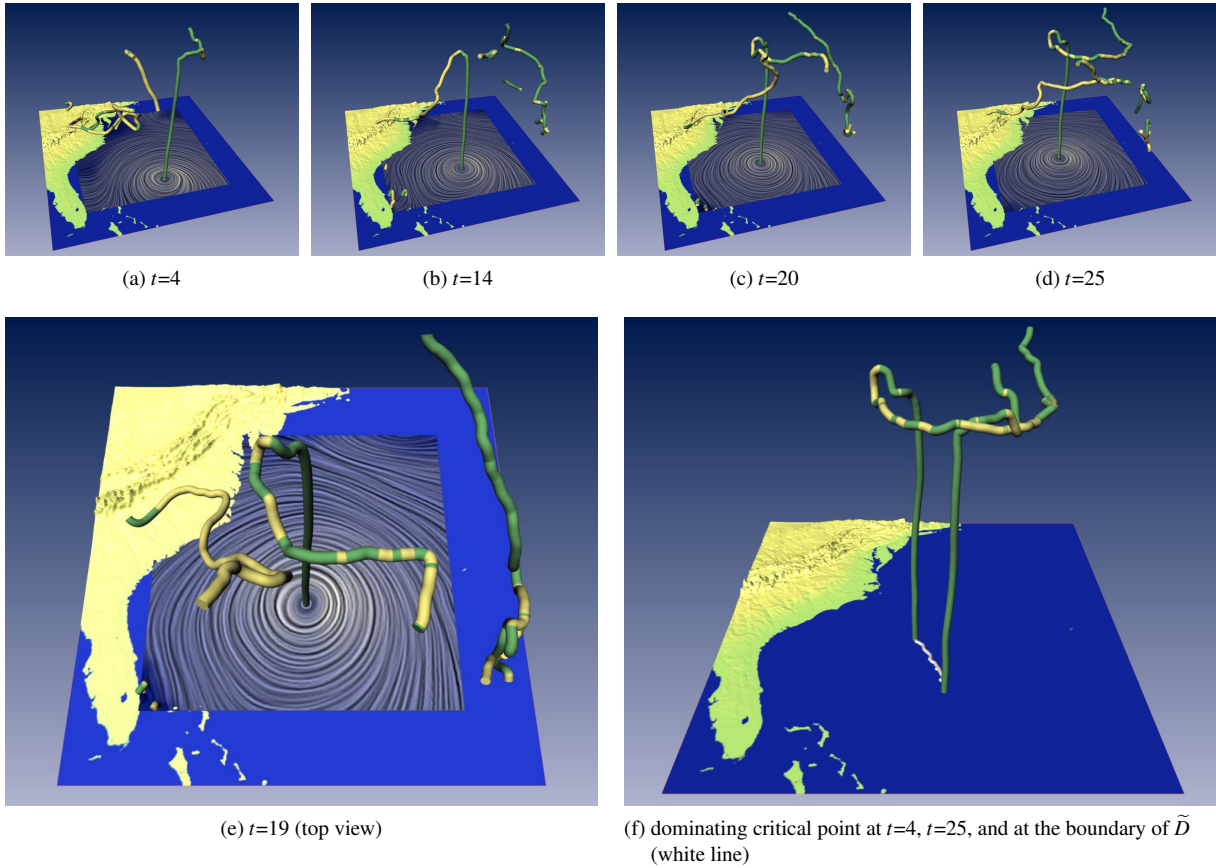


Figure 8: (x, y, s) -visualization of the Hurricane Isabel data set.

- [The02] THEISEL H.: Designing 2D vector fields of arbitrary topology. *Computer Graphics Forum (Eurographics 2002)* 21, 3 (2002), 595–604.
- [TRS03] THEISEL H., RÖSSL C., SEIDEL H.-P.: Compression of 2D vector fields under guaranteed topology preservation. *Computer Graphics Forum (Eurographics 2003)* 22, 3 (2003), 333–342.
- [TS03] THEISEL H., SEIDEL H.-P.: Feature flow fields. In *Data Visualization 2003. Proc. VisSym 03* (2003), pp. 141–148.
- [TSH01a] TRICOCHÉ X., SCHEUERMANN G., HAGEN H.: Continuous topology simplification of planar vector fields. In *Proc. Visualization 01* (2001), pp. 159–166.
- [TSH01b] TRICOCHÉ X., SCHEUERMANN G., HAGEN H.: Topology-based visualization of time-dependent 2D vector fields. In *Data Visualization 2001. Proc. VisSym 01* (2001), pp. 117–126.
- [TSW*05] THEISEL H., SAHNER J., WEINKAUFF T., HEGE H.-C., SEIDEL H.-P.: Extraction of parallel vector surfaces in 3d time-dependent fields and application to vortex core line tracking. In *Proc. IEEE Visualization 2005* (2005), pp. 631–638.
- [TWHS03] THEISEL H., WEINKAUFF T., HEGE H.-C., SEIDEL H.-P.: Saddle connectors - an approach to visualizing the topological skeleton of complex 3D vector fields. In *Proc. IEEE Visualization 2003* (2003), pp. 225–232.
- [TWHS05] THEISEL H., WEINKAUFF T., HEGE H.-C., SEIDEL H.-P.: Topological methods for 2D time-dependent vector fields based on stream lines and path lines. *IEEE Transactions on Visualization and Computer Graphics* 11, 4 (2005), 383–394.
- [WJE01] WESTERMANN R., JOHNSON C., ERTL T.: Topology-preserving smoothing of vector fields. *IEEE Transactions on Visualization and Computer Graphics* 7, 3 (2001), 222–229.
- [WS01] WISCHGOLL T., SCHEUERMANN G.: Detection and visualization of closed streamlines in planar flows. *IEEE Transactions on Visualization and Computer Graphics* 7, 2 (2001), 165–172.
- [WTHS04a] WEINKAUFF T., THEISEL H., HEGE H.-C., SEIDEL H.-P.: Boundary

switch connectors for topological visualization of complex 3D vector fields. In *Data Visualization 2004. Proc. VisSym 04* (2004), pp. 183–192.

[WTHS04b] WEINKAUFF T., THEISEL H., HEGE H.-C., SEIDEL H.-P.: Topological construction and visualization of higher order 3D vector fields. *Computer Graphics Forum (Eurographics 2004)* 23, 3 (2004), 469–478.

[WTHS05] WEINKAUFF T., THEISEL H., HEGE H.-C., SEIDEL H.-P.: Feature flow fields in out-of-core settings. In *Topo-In-Vis 2005* (2005), (submitted).

10. Appendix

To show that $\nabla \tilde{\mathbf{g}}$ at an s -fold bifurcation has eigenvalues of the structure $0, 0, -\sqrt{t_s}, \sqrt{t_s}$, we insert $\mathbf{v}_y = \lambda \mathbf{v}_x$ and $\mathbf{v}_t = \mu \mathbf{v}_x$ into the first order partials of $\tilde{\mathbf{g}}$. This gives

$$\tilde{\mathbf{g}}_x = \begin{pmatrix} \det(\mathbf{v}_x, \lambda \mathbf{v}_{xt} - \mu \mathbf{v}_{xy}) \\ \det(\mathbf{v}_x, \mu \mathbf{v}_{xx} - \mathbf{v}_{xt}) \\ 0 \\ \det(\mathbf{v}_x, \mathbf{v}_{xy} - \lambda \mathbf{v}_{xx}) \end{pmatrix}, \quad \tilde{\mathbf{g}}_y = \begin{pmatrix} \det(\mathbf{v}_x, \lambda \mathbf{v}_{yt} - \mu \mathbf{v}_{yy}) \\ \det(\mathbf{v}_x, \mu \mathbf{v}_{xy} - \mathbf{v}_{yt}) \\ 0 \\ \det(\mathbf{v}_x, \mathbf{v}_{yy} - \lambda \mathbf{v}_{xy}) \end{pmatrix},$$

$$\tilde{\mathbf{g}}_s = \begin{pmatrix} \det(\mathbf{v}_x, \lambda \mathbf{v}_{st} - \mu \mathbf{v}_{ys}) \\ \det(\mathbf{v}_x, \mu \mathbf{v}_{xs} - \mathbf{v}_{st}) \\ 0 \\ \det(\mathbf{v}_x, \mathbf{v}_{ys} - \lambda \mathbf{v}_{xs}) \end{pmatrix}, \quad \tilde{\mathbf{g}}_t = \begin{pmatrix} \det(\mathbf{v}_x, \lambda \mathbf{v}_{tt} - \mu \mathbf{v}_{tt}) \\ \det(\mathbf{v}_x, \mu \mathbf{v}_{tt} - \mathbf{v}_{tt}) \\ 0 \\ \det(\mathbf{v}_x, \mathbf{v}_{tt} - \lambda \mathbf{v}_{tt}) \end{pmatrix}.$$

The matrix $\nabla \tilde{\mathbf{g}} = (\tilde{\mathbf{g}}_x, \tilde{\mathbf{g}}_y, \tilde{\mathbf{g}}_s, \tilde{\mathbf{g}}_t)$ has rank 2 because for the third line of $\nabla \tilde{\mathbf{g}}$ we have $\nabla \tilde{\mathbf{g}}.3 = (0, 0, 0, 0)$, and for the remaining lines holds $\nabla \tilde{\mathbf{g}}.1 + \lambda \nabla \tilde{\mathbf{g}}.2 + \mu \nabla \tilde{\mathbf{g}}.4 = (0, 0, 0, 0)$. This gives two eigenvalues of 0. Since furthermore $\text{trace}(\nabla \tilde{\mathbf{g}}) = 0$, the remaining eigenvalues add to 0, yielding the eigenvalue structure $0, 0, -\sqrt{t_s}, \sqrt{t_s}$. In a similar way it can be shown that $\nabla \tilde{\mathbf{f}}$ has the eigenvalues $0, 0, -\sqrt{t_t}, \sqrt{t_t}$ at a t -fold bifurcation.